PCCP

RSC Publishing

PAPER

View Article Online
View Journal | View Issue

Cite this: *Phys. Chem. Chem. Phys.*, 2013, **15**, 13951

A parabolic model to control quantum interference in T-shaped molecular junctions

Daijiro Nozaki,*[a] Hâldun Sevinçli,[ab] Stanislav M. Avdoshenko,[ac] Rafael Gutierrez[a] and Gianaurelio Cuniberti[ad]

Received 18th December 2012,
Accepted 15th March 2013

DOI: 10.1039/c3cp44578j

www.rsc.org/pccp

Quantum interference (QI) effects in molecular devices have drawn increasing attention over the past years due to their unique features observed in the conductance spectrum. For the further development of single molecular devices exploiting QI effects, it is of great theoretical and practical interest to develop simple methods controlling the emergence and the positions of QI effects like anti-resonances or Fano line shapes in conductance spectra. In this work, starting from a well-known generic molecular junction with a side group (T-shaped molecule), we propose a simple graphical method to visualize the conditions for the appearance of quantum interference, Fano resonances or anti-resonances, in the conductance spectrum. By introducing a simple graphical representation (parabolic diagram), we can easily visualize the relation between the electronic parameters and the positions of normal resonant peaks and anti-resonant peaks induced by quantum interference in the conductance spectrum. This parabolic model not only can predict the emergence and energetic position of quantum interference from a few electronic parameters but also can enable one to know the coupling between the side group and the main conduction channel from measurements in the case of orthogonal basis. The results obtained within the parabolic model are validated using density-functional based quantum transport calculations in realistic T-shaped molecular junctions.

1. Introduction

Quantum interference (QI) effects in electron transport have been broadly studied in the field of mesoscopic physics,[1–5] and their appearance in molecular junctions has been suggested from studies on electron transfer.[6,7] In the context of charge transport in molecular devices, QI effects have drawn increasing attention over the past years due to their unique features observed in the conductance spectrum.[8–32] QI in molecular devices has vast applications such as molecular switches, molecular thermoelectric devices, molecular sensors, and molecular interferometers as shown in Fig. 1. For instance, since QI effects introduce additional dips in the conductance spectrum, it may be expected that they can considerably change the on/off ratios (Fig. 1(b)) and thermoelectric performance of molecular junctions (Fig. 1(c)).[21,26,32] Moreover, since it is possible to infer the molecular electronic structure as well as its topological connectivity from the analysis of transport line shapes, QI related effects might also be exploited for sensor (Fig. 1(d)) or interferometer applications (Fig. 1(e)) by monitoring the changes in the transmission spectrum as a function of *e.g.* a magnetic field.

It is therefore of great theoretical and practical interest to provide simple rules controlling the emergence of different types of QI effects like anti-resonances or Fano line shapes.[8,9,15,19] According to the lineshape, QI effects can manifest either as anti-resonances (negative, almost symmetric peaks) or as Fano resonances (asymmetric sharp peaks).[3,12–14] As a general qualitative trend, T-shaped[11,13–15,23,25–29] or cyclic molecules[16,29,31] tend to exhibit QI effects in their transmission spectra. Even the appearance of anti-resonance in the 1D linear chains exploiting non-orthogonality has been reported.[8,17,18]

Although many studies of QI effects have been conducted, the understanding of the origin of anti-resonances and Fano resonances in molecular junctions is still under debate. For further development of single molecular devices exploiting QI effects, the precise relationship between the electronic structure and QI-induced line shape in conductance spectra needs

[a] *Institute for Materials Science and Max Bergmann Center of Biomaterials, TU Dresden, 01062 Dresden, Germany. E-mail: daijiro.nozaki@gmail.com*
[b] *Department of Micro- and Nanotechnology (DTU Nanotech), Technical University of Denmark, DK-2800 Kgs. Lyngby, Denmark*
[c] *School of Materials Engineering, Purdue University, West Lafayette, Indiana 47907, USA*
[d] *Division of IT Convergence Engineering and National Center for Nanomaterials Technology, POSTECH, Pohang 790-784, Republic of Korea*

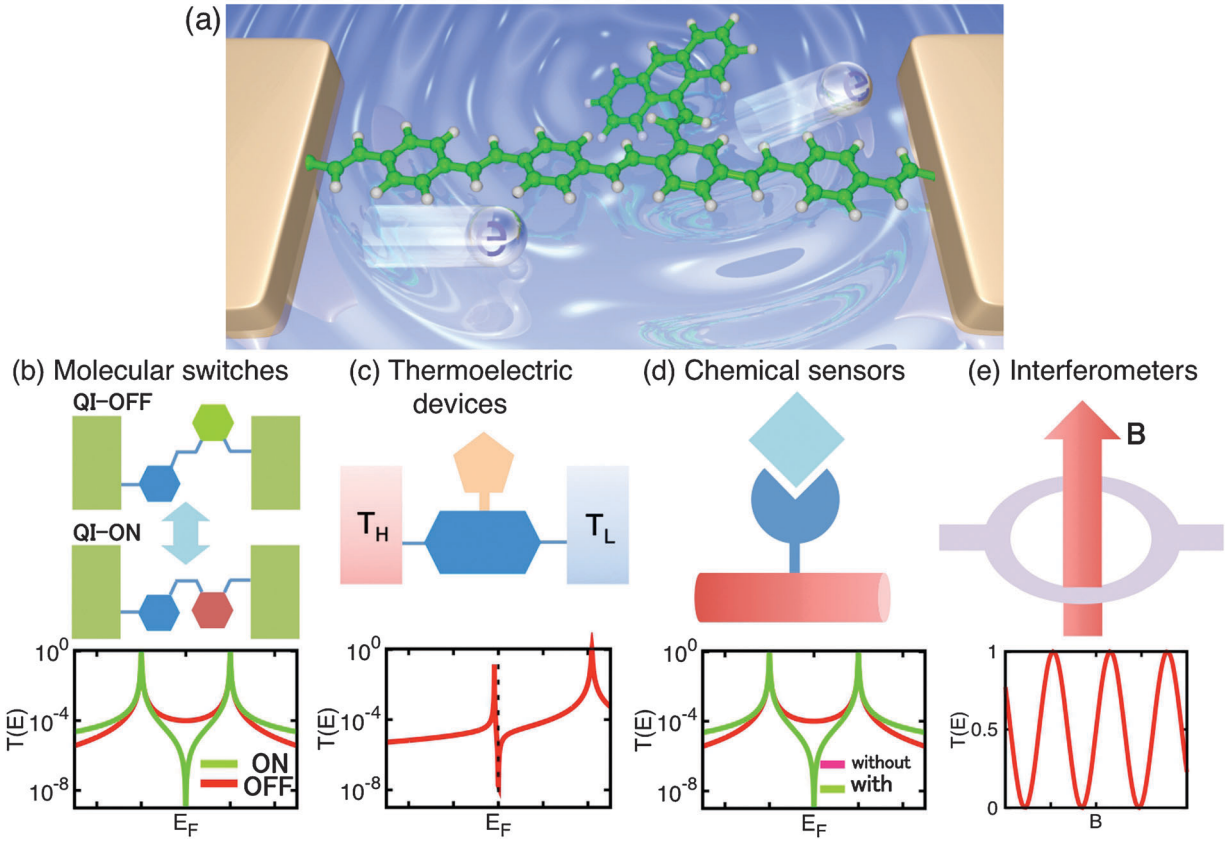

Fig. 1 Quantum interference (QI) in molecular junctions and their possible applications: (a) conceptual image of molecular devices exploiting quantum interference phenomena. A molecular wire with a single side group (T-shape molecule) is coupled between contacts. Electronic states in the side group interfere with the electron transport through the molecular wire. (b)–(e) Possible applications of quantum interference are shown. Since the QI effect causes abrupt drop in conductance spectra, it can be applied for (b) molecular switches, (c) thermoelectric devices, (d) QI-exploited chemical sensors, and (d) molecular interferometers.

to be understood. Although this can be achieved using extensive first-principles based calculations, it is also desirable to provide simple rules relating electronic structure and QI signatures in molecular scale systems.

Papadopoulos *et al.*[13] and Stadler and Markussen[26] have proposed simple and useful models to predict the appearance of the QI signatures of T-shaped junctions using two site approximation. In this work, at first we briefly review the conditions for the appearance of the two types of QI line shapes (anti-resonances and Fano resonances) in the transmission spectra of the T-shaped toy model. Then from the transmission formula in eqn (3), we propose a simple graphical method – called a parabolic diagram for simplicity, see Fig. 2(b) – to predict the type of QI effect and peak positions in transmission spectra in a graphical way without calculations of transmission function. In the second part of this study, we validate our parabolic model approach by computing on a first-principles basis the conductance of realistic molecular junctions with different side groups and displaying QI related features, finding a good quantitative agreement with the parabolic diagram approach. Since we assume that charges are transported through short molecular wires *via* a tunneling mechanism and that molecules are not weakly coupled to contacts but covalently connected to the contacts, the effect of Coulomb blockade can be negligible.[24]

2. Theoretical basis

2.1 Simple model of a T-shaped molecule

We start a generic molecular wire with a side group as schematically shown in Fig. 1(a). The system is attached to left and right contacts only through the central wire, *i.e.* the side groups do not directly couple to the contacts. The operator of the retarded Green's function G^r of the molecule attached to the contacts is given by[9,33]

$$G^r(E) = \sum_i \frac{|\psi_i\rangle\langle\psi_i|}{E + i\delta - \varepsilon_i}, \quad (1)$$

where $|\psi_i\rangle$ corresponds to the molecular orbital (MO) of the central molecule. Here, ε_i and $|\psi_i\rangle$ are the eigen-value and eigen-vector (both are complex) of H. H is a Hamiltonian for the whole system given by $H = H_M + \Sigma_L(E) + \Sigma_R(E)$, where H_M is a Hamiltonian for the central molecule and $\Sigma_{L/R}(E)$ are the self-energy terms due to the left/right contacts. If the energy spacing between the MOs is large enough for the broadening of the MOs due to the contacts ($\Delta\varepsilon_i \gg \mathrm{Im}[\varepsilon_i]$), the transmission through the system around energies $E \sim E_F$ is mainly affected by a few MOs around E since the contribution from deeper levels is expected to be small because of the large denominators in eqn (1). In this work we focus this case where coupling of the

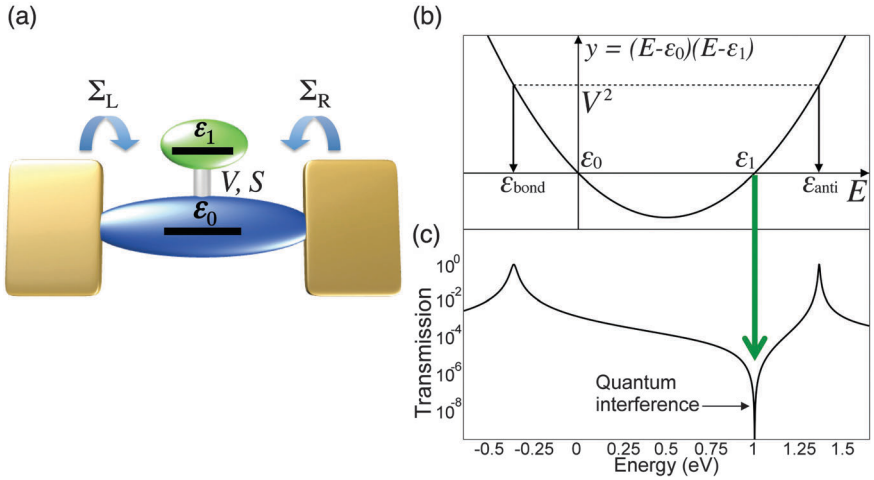

Fig. 2 (a) Schematic image of a molecular junction with a side group considered in this work. A molecule consisting of two fragments is coupled between contacts. The energies of two fragment molecular orbitals (MOs) are ε_0 and ε_1. The transfer integral and overlap matrix between them are given by V and S, respectively. $\Sigma_{L/R}$ represents the self-energies due to coupling to the left/right contacts. (b) Parabolic diagram showing the relation between on-site energies ε_0, ε_1 coupling V, and resonant peaks ε_{bond} and ε_{anti}. (c) The transmission function obtained from eqn (3) with $\varepsilon_0 = 0.0$ eV, $\varepsilon_1 = 1.0$ eV, $V^2 = 0.5$ eV^2, $S = 0$, and $\gamma = 0.01$ eV. The quantum interference effect is observed as a negative peak in the transmission spectrum. Its position and the shape of the transmission function can be predicted from the parabolic model in panel (b).

molecule to contacts is weak compared with energy spacing $\Delta\varepsilon_i$. As a result, as long as we focus on the transmission around these energies, charge transport in the model can be simplified to a well-known T-shaped two-site model in Fig. 2(a) as discussed in ref. 13 and 26. The energy ε_0 is for the central site and ε_1 for the side group. V and S are electronic coupling and overlap, respectively. Thus, Hamiltonian and overlap matrices for the molecule are given by

$$H_M = \begin{bmatrix} \varepsilon_0 & V \\ V & \varepsilon_1 \end{bmatrix}, \quad S_M = \begin{bmatrix} 1 & S \\ S & 1 \end{bmatrix}. \tag{2}$$

In real systems, ε_0 corresponds to one of the frontier fragment MOs, which is delocalized over the main chain and is responsible for charge transport, while ε_1 corresponds to fragment MOs of the side group, which have the strongest coupling with the ε_0 states. Some molecular wires show QI due to the topology of molecular wires,[9,19] but we assume that the state ε_0 delocalized over the main chain establishes a normal resonant conduction.

Within Landauer's theory,[33] the transmission function of the T-shaped toy model can be computed *via* $T(E) = \mathrm{Tr}[G^r(E)\Gamma_L(E)G^a(E)\Gamma_R(E)]$, where $\Gamma_{L/R}(E)$ correspond to the spectral densities of the electrodes. Here we use an orthogonal expression ($S = 0$) in ref. 13 and 26. The extension to the non-orthogonal case ($S \neq 0$) is shown later. Since the coupling to the electrodes and to the side group can be represented by three self energies $\Sigma_{L/R}(E)$ and $\Sigma_S(E) = V^2/(E - \varepsilon_1)$,[34] the retarded Green's function of the molecular junction in the orthogonal basis can be written as: $[G^r(E)]^{-1} = (E + i\delta) - \varepsilon_0 - \Sigma_L(E) - \Sigma_R(E) - V^2/(E - \varepsilon_1)$.

Energy dependence of the self-energy can be a factor controlling the quantum interference in molecular junctions. In addition, place of contacts could also be influential.[9] However, the main focus of this study is the controlling of QI in a T-shaped molecule by tuning electronic parameters of the molecular wires, thus it is out of scope of this work. If we neglect the energy dependence of the electrode self-energies within the wide-band limit (WBL) for simplicity, the contribution of the reservoirs can be written as $\Sigma_{L/R}(E) = -i\gamma_{L/R}$.[34] The broadening $\Gamma_{L/R}(E)$ functions are then defined as $\Gamma_{L/R}(E) = i[\Gamma_{L/R} - \Gamma_{L/R}^{\dagger}] = 2\gamma_{L/R}$. Hereafter we assume $\gamma_{L/R} = \gamma$. The transmission function of the T-shaped toy model is then simply given by:[13,26]

$$T(E) = \frac{4\gamma^2}{\left(E - \varepsilon_0 - \dfrac{V^2}{E - \varepsilon_1}\right)^2 + 4\gamma^2}, \tag{3}$$

From eqn (3), it is obvious that when the term $(E - \varepsilon_0 - V^2/(E - \varepsilon_1))^2$ is a minimum, $T(E)$ attains its maximum. This is a Breit–Wigner (BW)-type resonant peak with width γ. The positions of the peaks are given by the solutions of the quadratic equation:

$$(E - \varepsilon_0)(E - \varepsilon_1) - V^2 = 0, \tag{4}$$

with solutions ε_{bond}, ε_{anti} given by

$$\varepsilon_{bond/anti} = \frac{\varepsilon_0 + \varepsilon_1 \pm \sqrt{(\varepsilon_0 - \varepsilon_1)^2 + 4V^2}}{2}, \tag{5}$$

where the transmission maxima take place.[13,14,26] On the other hand, the system gives a dip at $E = \varepsilon_1$ with $T(E) = 0$, since the denominator in eqn (3) diverges, $\lim_{E \to \varepsilon_1 \pm 0} V^2/(E - \varepsilon_1) = \pm\infty$.[13,26,29] At this point we propose a graphical representation (parabolic diagram) by plotting the variable $y = (E - \varepsilon_0)(E - \varepsilon_1)$ as a function of the energy E, as shown in Fig. 2(b). Using this diagram, the peak and dip positions in transmission spectra as well as their relation to the relevant electronic parameters ε_{bond}, ε_{anti}, ε_0, V, and ε_1 can easily be visualized.

Although the conditions for Fano resonance and anti-resonance are also shown using a two site model in ref. 26,

from this parabolic model we can see that (i) when $|\varepsilon_0 - \varepsilon_1|/|V|$ is small, an anti-resonance appears at $E = \varepsilon_1$, with two symmetric resonance peaks at $E = \varepsilon_{\text{bond}}$ and $E = \varepsilon_{\text{anti}}$, since the two resonant peaks get apart energetically with increasing $|V|$ or decreasing $|\varepsilon_0 - \varepsilon_1|$. We can also see that (ii) when $|\varepsilon_0 - \varepsilon_1|/|V|$ is large, the system presents asymmetric Fano line shapes since smaller $|V|$ or larger $|\varepsilon_0 - \varepsilon_1|$ makes a dip and a peak closer in energy. Interestingly, when ε_0 is equal to ε_1, this system does not show sharp Fano resonance. This is because the two resonant peaks converge to a single peak in the weak coupling limit of V.

The usefulness of our parabolic model is that once given a few key electronic parameters (ε_0, ε_1, and V), the energetic position of positive resonance peaks ($E = \varepsilon_{\text{bond}}$, $\varepsilon_{\text{anti}}$) and negative peaks ($E = \varepsilon_1$) in $T(E)$ can be estimated from the parabolic diagram in Fig. 2(b) *without* explicitly computing the transmission function from eqn (3) and (6) or by using more sophisticated numerical methods.

To illustrate this point further, if one would like to examine the QI effects of molecular wires having *e.g.* a conducting fragment MO at $\varepsilon_0 = 0.0$ eV and a localized fragment MO at $\varepsilon_1 = 1.0$ eV with coupling $V^2 = 0.5$ eV^2, it is possible to estimate the position of the BW-type resonance and of an anti-resonance by drawing the parabola as in Fig. 2(b) without using the formula in eqn (3). Fig. 2(c) presents the transmission function calculated from eqn (3) using the same parameters. We can see that the position of the negative and positive peaks completely matches with the features of the parabolic diagram. More interestingly, it is also possible to estimate the coupling V from the position of the positive and negative peaks in the transmission function using this parabolic diagram. If the peak ($\varepsilon_{\text{bond/anti}}$) and dip ($\varepsilon_1$) positions can be resolved experimentally, the on-site energy (ε_0) and the electronic coupling (V) are uniquely determined from the parabolic model. First, the on-site energy (ε_0) is easily obtained from the centre of the parabola since $(\varepsilon_0 + \varepsilon_1)/2 = (\varepsilon_{\text{bond}} + \varepsilon_{\text{anti}})/2$. Then, V is obtained by $V^2 = (\varepsilon_{\text{anti}} - \varepsilon_0)(\varepsilon_{\text{anti}} - \varepsilon_1)$ or $V^2 = (\varepsilon_{\text{bond}} - \varepsilon_0)(\varepsilon_{\text{bond}} - \varepsilon_1)$.

Note that the anti-resonance peaks can be realized in non-T-shaped molecules[8,9,17–19] when the summation of Green's function in eqn (1) equals zero, or when the non-orthogonality is exploited,[8,17,18] or when the topology of electronic structure can be modeled as shown in Fig. 2(a) after the transformation of the basis such as Löwdin transformation and localized molecular orbital methods.[23,24] In any basis set, as long as the Hamiltonian of the molecular system can be projected in the topology of the T-shape as shown in Fig. 2(b), we can apply the parabolic model to estimate the transmission function using eqn (3) and (6). Thus, the shape of the molecule does not always need to be T-shaped. However, the advantage to use T-shaped molecules lies in the controllability of the negative peaks. Since the state ε_1 of the side group always contributes to the negative peak because of the divergence of Σ_s at $E = \varepsilon_1$,[13,26,29] the position of the negative peak can be easily tuned by simply changing the molecular structure of the side groups. In addition, the coupling V can also be tuned by linkers. Thus, we restrict our interest in T-shaped molecular structure in this study.

Finally we derive the transmission function of the T-shaped toy model in non-orthogonal basis within WBL, which is not derived in ref. 13 and 26. In the case of a non-orthogonal basis ($S \neq 0$), the term $\Sigma_s = V^2/(E - \varepsilon_1)$ is replaced by $\Sigma_s = (ES - V)^2/(E - \varepsilon_1)$. Then, the term $-V^2$ in eqn (3) becomes $-(ES - V)^2$, thus the dotted flat lines in Fig. 2(b) meaning $y = V^2$ are replaced by shallow parabolas, $y = (ES - V)^2$. The two solutions $\varepsilon_{\text{bond}}$ and $\varepsilon_{\text{anti}}$ in the non-orthogonal basis are given by intersections between $y = (E - \varepsilon_0)(E - \varepsilon_1)$ and $y = (ES - V)^2$. The transmission function of two site approximation of T-shape molecules within WBL in non-orthogonal basis is given by

$$T(E) = \frac{4\gamma^2}{\left(E - \varepsilon_0 - \dfrac{(ES - V)^2}{E - \varepsilon_1}\right)^2 + 4\gamma^2}, \qquad (6)$$

We used this function for the calculation of transmission as a toy model in the next section. In the case of non-orthogonal basis, it is impossible to determine the key parameters (ε_0, S, V) from the positions of peaks and a dip from measured transmission spectra since there are three unknown parameters (ε_0, S, V) to the two simultaneous equations; $y = (E - \varepsilon_0)(E - \varepsilon_1)$ and $y = (ES - V)^2$.

3. Applications

3.1 Remarks on realistic calculations

In order to demonstrate the relevance of the parabolic diagram for realistic systems, we have designed two molecular wires with side groups as shown in Fig. 3, which display Fano resonances and anti-resonances. We call them model A and model B.

First, we have analyzed the electronic structures of the T-shaped molecules in the gas phase using the fragment molecular orbital (FMO) method.[35] Then we have predicted whether the modeled systems satisfy the conditions for Fano and anti-resonances using the parabolic model and the non-orthogonal version of the simple toy model. Finally we confirmed the prediction by calculating the transmission functions using a density functional based approach. As electrodes, we chose hydrogen terminated semi-infinite Si(111) slabs. We used the gDFTB program[36] for the transmission calculations, which is based on a density-functional tight binding method.[37] In order to release strains between the side groups and the main chain, and between the molecular wires and the electrodes,[38,39] all transmission calculations were performed after structure relaxation in the same way as in ref. 40 using a minimal basis set for all of the atoms.[41] Although water molecules or other impurities could be present around the molecular junctions, we omit them for simplicity.

3.2 Analysis of fragment molecular orbitals

Firstly, in order to generate a Fano resonance, a side-group needs to be weakly coupled with the main chain such that the energy level of the eigen-state responsible for the conduction (ε_0) is separated enough from that of the localized

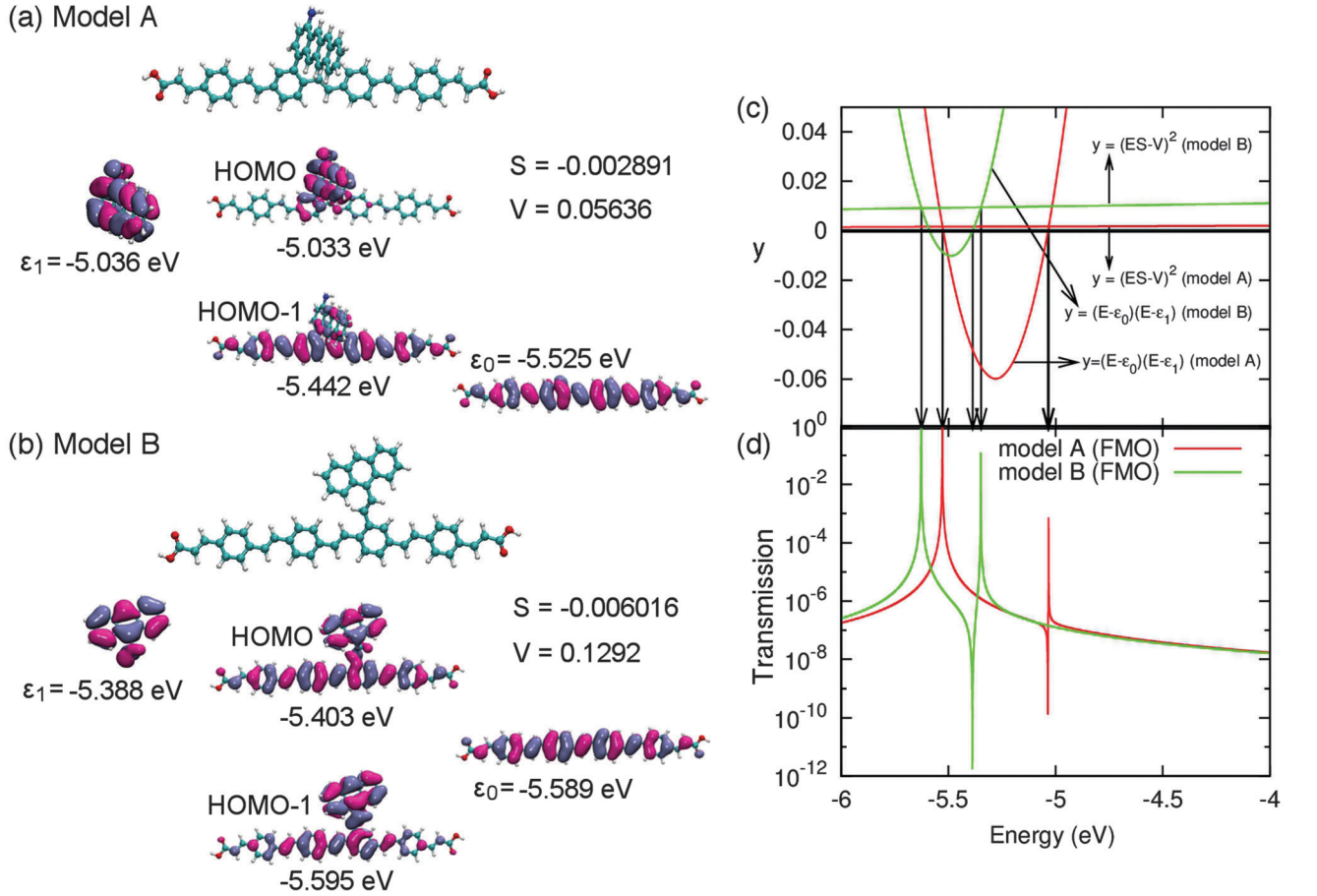

Fig. 3 (a) and (b) FMO analysis of the two T-shaped molecular wires modeled for the demonstration of Fano and anti-resonances. Model A has a vertically grafted side functional group, while model B has a side group connected by an sp^2 unsaturated linker. In the middle, HOMO and HOMO − 1 of the models A and B are shown with their energy levels. Fragment MOs (HOMOs) of the side groups are shown on the left side with their energies and fragment MOs of the main chains with their energies on the right side. Transfer integrals and overlaps between them are shown on the top right. (c) Parabolic diagram for the model A and model B. Parameters (ε_0, ε_1, S, V) are taken from FMO analysis in panels (a) and (b). We can speculate the peaks and dips in the transmission spectra from this diagram without calculating transmission functions. (d) Transmission spectra calculated from a non-orthogonal version of the 2-site toy model (eqn (6)). γ is set to 0.1 meV. Since the model A has the large value of $|\varepsilon_0 - \varepsilon_1|/|V| = 8.68$, sharp Fano resonance is observed in the 2-site toy model calculation for the model A.

fragment MO at the side group (ε_1). For this requirement, we built model A by grafting the side group (thetrathene-derivative) vertically to the main chain consisting of *p*-phenylene vinylene (PPV). This is how π–π interaction between them can be weakened.

Next, in order to generate an anti-resonance, we built model B by strongly coupling a side-group to the main chain such that the energy level ε_0 is close to ε_1. For strong electronic coupling between them, the side group is linked to the main chain using an unsaturated sp^2 linker.

After the relaxation of models A and B, each T-shaped molecule in the gas phase was divided into two fragments. Then, the eigenvalues of each fragment and coupling between them were calculated using the FMO method[35] to estimate the coupling strength V, overlap S, and how one of the eigen-states responsible for the conduction (ε_0) is energetically separated from that of the localized fragment MO at the side group (ε_1). In this study, we focused on the energy range around frontier orbitals, thus the energy level of the HOMO of the side fragment was chosen as ε_1 and that of the HOMO of the main chain moiety was chosen as ε_0.

The results of FMO analysis for the model A are presented in Fig. 3(a). We can see that both of the overlap S and the coupling V are small in model A because of the twisted grafting of the side group to the main chain. In addition to the small S and V, the energy difference between ε_1 and ε_0 is large. Note also that the side group retains a localized orbital (see the HOMO of model A). Therefore, we can expect that model A manifests a Fano resonance in the transmission spectrum. On the other hand, from the FMO analysis of the model B in Fig. 3(b), we can see that the energy difference between ε_1 and ε_0 is small and that S and V are large. Because of these large S and V, fragment MOs are hybridized after coupling and the side group no longer retains localized states (see the delocalized HOMO and HOMO − 1 of model B). Therefore, we can expect that the anti-resonance appears from the model B.

It is reasonable to verify these expectations from the parabolic model and further to confirm from the non-orthogonal

version of the T-shaped toy model. For this purpose, we depicted the corresponding parabolic diagrams for both models A and B to estimate the line shape of transmission spectra in Fig 3(c). The parameters (ε_1, ε_0, S, and V) are taken from the FMO analysis in Fig. 3(a) and (b). We can see that the energy of the side group (ε_1) yielding the anti-resonance and one of the intersections between $y = (E - \varepsilon_0)(E - \varepsilon_1)$ and $y = (ES - V)^2$ around $E = -5.0$ eV are close to each other in model A. On the other hand, in model B, they are not close enough. From these diagrams we can expect the Fano resonance from model A and solely anti-resonance from B around $E = \varepsilon_1$. In order to confirm these expectations from the parabolic diagrams, we have calculated transmission spectra using the non-orthogonal version of the 2-site toy model in eqn (6). Fig. 3(d) presents transmission spectra of the models A and B. As expected from the parabolic model, we can see Fano resonance in model A and anti-resonance in model B.

3.3 Validation of the parabolic diagram: first-principles transport calculations

As a further validation of the prediction deduced from the FMO analysis of model systems in the gas phase with the parabolic diagram and the toy model in the previous subsection, we connected the modeled systems between contacts and calculated the transmission spectra using a first principles transport calculation method[36] (gDFTB). We used carboxylic acids for the linkers connecting between the T-shaped molecule and the Si contacts.

Fig. 4 summarizes the transmission and total (DOS) and projected DOS (PDOS) plots of the modeled systems. In the absence of

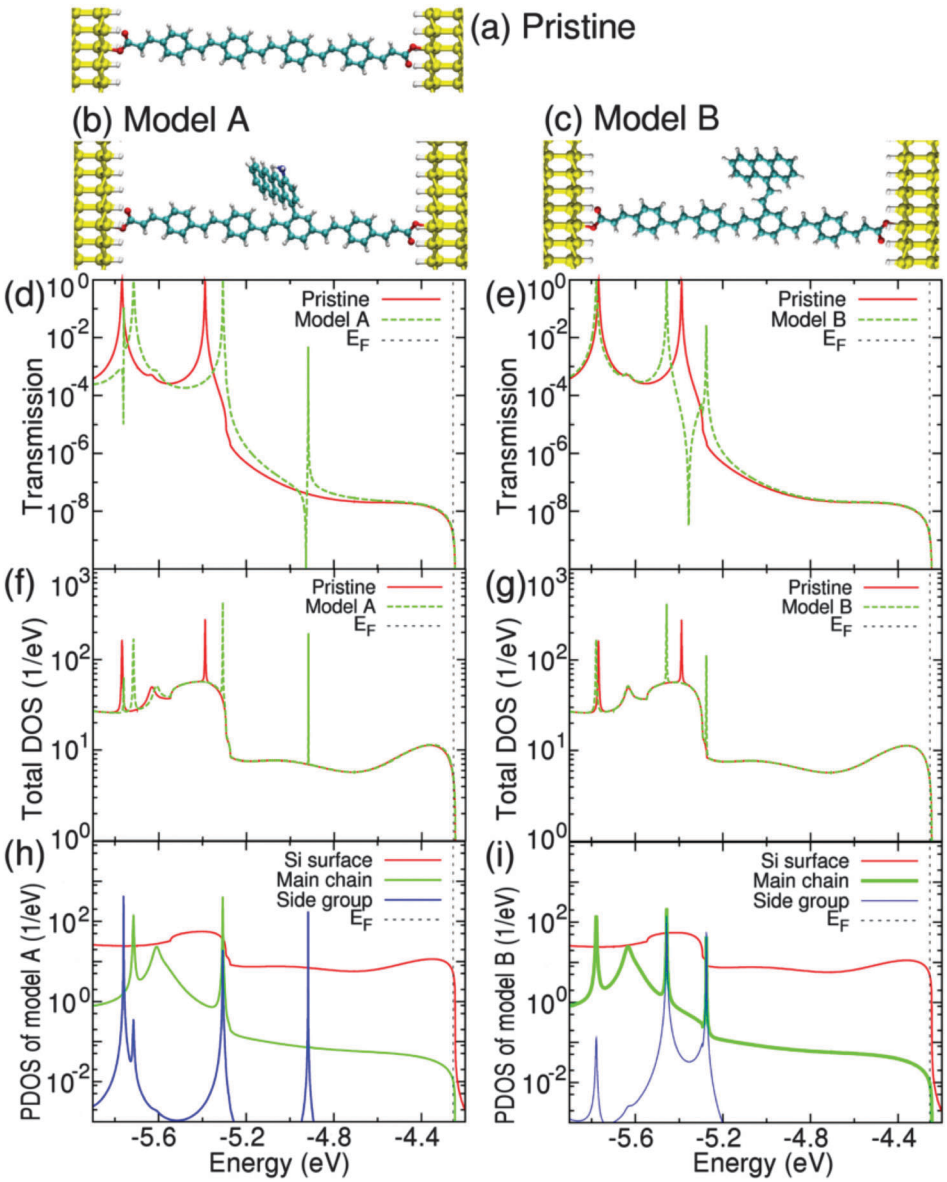

Fig. 4 Demonstration of Fano resonance (left panels) and anti-resonance (right panels).

the side group, the region with low transmission spreads from the HOMO to the Fermi energy. From this peak around $E = -5.4$ eV, the aforementioned assumption that the main chain establishes normal resonance through the delocalized state is validated. In the presence of the side group, a Fano resonance appears around $E = -4.9$ eV (green line in Fig. 4(d)) in model A due to the interference between the localized state from the side group and the conduction state as expected from the parabolic model and the toy model analysis in Section 3.2. We can clearly see the localized state around $E = -4.9$ eV originating from the side group in the PDOS plot (blue line) in Fig. 4(h).

As for the model B, we can see that the resonant peak of the pristine system at -5.4 eV (red line in Fig. 4(e)) splits into bonding and anti-bonding peaks after the attachment of the side group because of the strong electronic interaction between the side group and the main chain (see green lines in Fig. 4(e) and (g)). The transmission of model B gives an anti-resonance peak between the bonding and anti bonding peaks as expected from the parabolic model and the toy model analysis in Section 3.2. From the PDOS plot in Fig. 4(i), it is clear that the states of the side group are not localized anymore (thus not satisfying the conditions for Fano resonance) but delocalized with the main chain because of the strong electronic interaction between the side group and the main chain.

4. Conclusions

We have developed a simple graphical model to predict the appearance and the positions of the quantum interference in transmission spectra in the T-shaped molecular junctions. By introducing a parabolic diagram, the relationship between key electronic parameters and the line shape of the transmission spectra can be visualized without calculating transmission functions. We have demonstrated two types of quantum interference phenomena, Fano and anti-resonances in transmission spectra using the parabolic model with the T-shaped toy model. Our prediction with those models was validated for realistic T-shaped molecular junctions using first-principles transport calculations. Thus, the parabolic model potentially allows for tailoring the molecular system presenting Fano- or anti-resonance as desired. Our results are expected to provide very helpful guidelines for building functional molecular devices which exploit QI effects.

Acknowledgements

We gratefully acknowledge support from the German Excellence Initiative *via* the Cluster of Excellence EXC 1056 ''Center for Advancing Electronics Dresden'' (cfAED). We also gratefully acknowledge for the funds from the European Union (ERDF) and the Free State of Saxony *via* TP A2 (''MolFunc'') of the cluster of excellence ''European Center for Emerging Materials and Processes Dresden'' (ECEMP), from the European Union (ERDF) and the Free State of Saxony *via* the ESF project 080942409 InnovaSens, and from World Class University program funded by the Ministry of Education, Science and Technology through the National Research Foundation of Korea (R31-10100). We acknowledge the Center for Information Services and High Performance Computing (ZIH) at the Dresden University of Technology for computational resources.

Notes and references

1 E. Akkermans and G. Montambaux, *Mesoscopic Physics of Electrons and Photons*, Cambridge University Press, Cambridge, 2007.
2 J. L. D'Amato, H. M. Pastawski and J. F. Weisz, *Phys. Rev. B: Condens. Matter Mater. Phys.*, 1989, **39**, 3554.
3 M. L. Ladrón de Guevara, F. Claro and P. A. Orellana, *Phys. Rev. B: Condens. Matter Mater. Phys.*, 2003, **67**, 195335.
4 K. Kang, S. Y. Cho, J.-J. Kim and S.-C. Shin, *Phys. Rev. B: Condens. Matter Mater. Phys.*, 2001, **63**, 113304.
5 M. Sato, H. Aikawa, K. Kobayashi, S. Katsumoto and Y. Iye, *Phys. Rev. Lett.*, 2005, **95**, 066801.
6 P. R. Levstein, H. M. Pastawski and J. L. D'Amato, *J. Phys.: Condens. Matter*, 1990, **2**, 1781.
7 M. A. Ratner, *J. Phys. Chem.*, 1990, **94**, 4877.
8 E. G. Emberly and G. Kirczenow, *J. Phys.: Condens. Matter*, 1999, **11**, 6911.
9 T. Tada and K. Yoshizawa, *ChemPhysChem*, 2002, **3**, 1035.
10 K. Walczak, *Cent. Eur. J. Chem.*, 2004, **2**, 524.
11 J. Barański and T. Domański, *Phys. Rev. B: Condens. Matter Mater. Phys.*, 2011, **84**, 195424.
12 K. Sasada and N. Hatano, *Physica E*, 2005, **29**, 609.
13 T. A. Papadopoulos, I. M. Grace and C. J. Lambert, *Phys. Rev. B: Condens. Matter Mater. Phys.*, 2006, **74**, 193306.
14 A. Kormányos, I. Grace and C. J. Lambert, *Phys. Rev. B: Condens. Matter Mater. Phys.*, 2009, **79**, 075119.
15 G. C. Solomon, D. Q. Andrews, R. P. Van Duyne and M. A. Ratner, *J. Am. Chem. Soc.*, 2008, **130**, 7788.
16 J. Rincón, K. Hallberg, A. A. Aligia and S. Ramasesha, *Phys. Rev. Lett.*, 2009, **103**, 266807.
17 E. G. Emberly and G. Kirczenow, *Phys. Rev. Lett.*, 1998, **81**, 5205.
18 S. T. Rittenhouse and B. L. Johnson, *Phys. Rev. B: Condens. Matter Mater. Phys.*, 2005, **71**, 035118.
19 T. Markussen, R. Stadler and K. S. Thygesen, *Nano Lett.*, 2010, **10**, 4260.
20 T. Markussen, R. Stadler and K. S. Thygesen, *Phys. Chem. Chem. Phys.*, 2011, **13**, 14311.
21 J. P. Bergfield, G. C. Solomon, C. A. Stafford and M. A. Ratner, *Nano Lett.*, 2011, **11**, 2759.
22 J. P. Bergfield and C. A. Stafford, *Nano Lett.*, 2009, **9**, 3072.
23 T. Markussen, J. Schiötz and K. S. Thygesen, *J. Chem. Phys.*, 2010, **132**, 224104.
24 C. M. Guédon, H. Valkenier, T. Markussen, K. S. Thygesen, J. C. Hummelen and S. J. van der Molen, *Nat. Nanotechnol.*, 2012, **7**, 305.
25 G. C. Solomon, J. P. Bergfield, C. A. Stafford and M. A. Ratner, *Beilstein J. Nanotechnol.*, 2011, **2**, 862.
26 R. Stadler and T. Markussen, *J. Chem. Phys.*, 2011, **135**, 154109.

27 G. C. Solomon, D. Q. Andrew, T. Hansen, R. H. Goldsmith, M. R. Wasielewski, R. P. Van Duyne and M. A. Ratner, *J. Chem. Phys.*, 2008, **129**, 054701.
28 C. A. Stafford, D. M. Cardamone and S. Mazmudar, *Nanotechnology*, 2012, **18**, 424014.
29 T. Hansen, G. C. Solomon, D. Q. Andrews and M. A. Ratner, *J. Chem. Phys.*, 2009, **131**, 194704.
30 R. E. Sparks, V. M. García-Suárez, D. Zs. Manrique and C. J. Lambert, *Phys. Rev. B: Condens. Matter Mater. Phys.*, 2011, **83**, 075437.
31 D. A. Lovey and R. H. Romero, *Chem. Phys. Lett.*, 2012, **530**, 86.
32 P. Trocha and J. Barnaś, *Phys. Rev. B: Condens. Matter Mater. Phys.*, 2012, **85**, 085408.
33 S. Datta, *Electronic Transport in Mesoscopic Systems*, Cambridge University Press, Cambridge, 1995.
34 Energy-dependence of self-energy $\Sigma_{L/R}(E)$ is introduced as follows. When the energy dependent self-energy terms for the left/right contacts are defined as $\Sigma_{L/R}(E) = \eta(E) + i\gamma(E) = \mathrm{Re}[\Sigma_{L/R}(E)] + i\,\mathrm{Im}[\Sigma_{L/R}(E)]$, the terms of ε_0 and γ in eqn (3) are corrected to $\varepsilon_0 \rightarrow \varepsilon_0 + 2\eta(E)$ and $\gamma \rightarrow \gamma(E)$, respectively. Then, the parabolic equation in Fig. 2(b) is modified as $y = (E - \varepsilon_{0,\mathrm{eff}})(E - \varepsilon_1)$, where $\varepsilon_{0,\mathrm{eff}}$ includes the shift of ε_0 due to the real part of the self-energy term as $\varepsilon_{0,\mathrm{eff}} = \varepsilon_0 + 2\eta(E)$. The term $\gamma(E)$ only contributes to broadening of spectra, thus it does not affect the position of the anti-resonance peak. Although the peak positions of Breit–Wigner resonances ($\varepsilon_{\mathrm{bond}}$, $\varepsilon_{\mathrm{anti}}$) will be shifted due to $\eta(E)$, the condition to realize Fano resonance that $|\varepsilon_0 - \varepsilon_1|/|V|$ being large is not changed.
35 K. Kitaura, E. Ikeo, T. Asada, T. Nakano and M. Uebayasi, *Chem. Phys. Lett.*, 1999, **313**, 701.
36 A. Pecchia, G. Penazzi, L. Salvucci and A. Di Carlo, *New J. Phys.*, 2008, **10**, 065022.
37 http://www.dftb.org.
38 C. Q. Sun, *Prog. Mater. Sci.*, 2009, **54**, 179.
39 W. Zheng and C. Q. Sun, *Energy Environ. Sci.*, 2011, **4**, 627.
40 D. Nozaki and G. Cuniberti, *Nano Res.*, 2009, **2**, 648.
41 C. Köhler, Z. Hajnal, P. Deák, Th. Frauenheim and S. Suhai, *Phys. Rev. B: Condens. Matter Mater. Phys.*, 2001, **64**, 085333.

